Direct Evidence for Local Symmetry Breaking during a Strain Glass Transition

Yumei Zhou,[1] Dezhen Xue,[1,*] Ya Tian,[1] Xiangdong Ding,[1,†] Shengwu Guo,[1] Kazuhiro Otsuka,[2] Jun Sun,[1] and Xiaobing Ren[1,2,‡]

[1]*Multi-disciplinary Materials Research Center, Frontier Institute of Science and Technology, State Key Laboratory*
for Mechanical Behavior of Materials, Xi'an Jiaotong University, Xi'an 710049, China
[2]*Ferroic Physics Group, National Institute for Materials Science, Tsukuba, 305-0047 Ibaraki, Japan*
(Received 12 July 2013; published 16 January 2014)

Strain glass transition is a unique nanoscale displacive transition with local symmetry breaking while maintaining the macroscopic symmetry or average structure unchanged. It usually occurs in the "nonmartensitic" composition range of a martensitic system. So far, only indirect evidence exists for such a transition, essentially from macroscopic measurements and low-resolution transmission electron microscopy observations, and there is a lack of direct evidence for the speculated local symmetry breaking and the sluggish nature of the glass transition. In this Letter we report *in situ* high-resolution transmission electron microscopy observations on a $Ti_{50}(Pd_{41}Cr_9)$ strain glass alloy and direct evidence for these key issues. Our results show that at temperatures well above the strain glass transition temperature (T_g), the lattice is essentially an undistorted $B2$ structure. With approaching T_g, the local symmetry breaking gradually occurs with the formation and growth of nanomartensite clusters with a combined stacking period of three and four plane intervals, but the average structure measured by x-ray diffraction remains $B2$. These nanomartensite clusters become finally frozen below T_g. Our results provide not only a microscopic basis for the macroscopic properties of strain glass, but also new insights into a range of possible applications of this unique class of materials.

Phase transitions in ferroic materials break the symmetry of their respective Hamiltonians, and thereby are characterized by an order parameter [1,2]. For martensitic or ferroelastic transitions in shape memory alloys (SMAs), such symmetry breaking produces the spontaneous strain (ε) as the order parameter [2]. Below the transition temperature, the low symmetry violates the ergodicity of the system by limiting the phase space to either the $+\varepsilon$ or the $-\varepsilon$ [2]. The variation of ε with temperature and stress field leads to the shape memory effect (SME) and superelasticity (SE), which have numerous applications in devices ranging from actuators to sensors [3].

Recently, strain glass transition was found in "nonmartensitic" composition range of a martensitic system [4]. It is considered to be a unique nanoscale displacive transition with local symmetry breaking while maintaining the macroscopic symmetry or average structure unchanged [4–9]. The concept of strain glass is not only of potential interest for applications such as the unexpected shape memory effect and superelasticity of the nonmartensitic system [7] and stress tuned intelligent damping properties [10], but also provides insights into long-standing puzzles on the zero thermal expansion behavior of invar alloys [11]. However, up to now, there exists only indirect evidence for such a transition, essentially from macroscopic measurements and low-resolution transmission electron microscopy (TEM) observations [4,6,7,12,13]. For instance, it exhibits important glass transition features on the mechanical signals, such as the dynamic freezing measured by dynamic mechanical analysis (DMA) experiments [12,13], and the breaking down of ergodicity

measured by zero-field-cooling and field-cooling (ZFC/FC) experiments [6]. Furthermore, it maintains the parent phase $B2$ symmetry over the whole temperature range as observed by *in situ* x-ray diffractometry (XRD) [12]. Besides, several numerical simulations and theoretical models in the presence of disorder also have been proposed to investigate this kind of nanoscale displacive transition [5,14–17]. As the freezing process of the strain glass transition is manifested by the mechanical signals, strain glass is supposed to be a frozen state of local lattice strains, where the local symmetry is broken [5]. Based on this consideration, the preliminary understanding on the occurrence of strain glass is linked to the existence of point defects. Because of the site randomness of point defects and competition between various localized strain variants with similar ground state energy, the system freezes into a strain glass state with local strain ordering [4].

However, there is a lack of direct evidence for the above speculated local strain ordering and the local symmetry breaking. Previous studies using low-resolution TEM revealed only the existence of nanosized domains, but the local structure within these nanodomains remains a puzzle [4]. On the other hand, despite these indirect evidences for the freezing process of strain glass transition by measuring macroscopic properties (DMA, ZFC/FC, XRD) [4,6,7,12,13], the direct observation of such a freezing process at the atomic scale is still missing. Therefore, the direct observation by high-resolution transmission electron microscopy (HREM) is thus of great interest and is expected to provide a microscopic basis for the glass behaviors observed in macroscopic experiments.

In this Letter, we therefore performed *in situ* HREM observations on a $Ti_{50}(Pd_{41}Cr_9)$ alloy [13], locating in the strain glass region in the temperature-composition phase diagram as marked by the arrow in Fig. 1(a). Figure 1(b) shows that it exhibits a frequency-dependent dip at a critical temperature (glass transition temperature T_g) in the storage modulus (inverse of the mechanical susceptibility $d\varepsilon/d\sigma$) together with a frequency-dependent peak in internal friction ($\tan\delta$). The frequency dependence of $T_g(\omega)$ obeys a Vogel–Fulcher relation $\omega = \omega_0 \exp[-E_a/k_B(T_g - T_0)]$, as shown in the inset of Fig. 1(b) [1], and the fitting yields an ideal freezing temperature T_0 (T_g at 0 Hz) of 298 K, which ensures the alloy to be in the strain glass state at room temperature (293 K). Figure 1(c) shows that no obvious endothermic or exothermic peak could be observed in the heat flow curve and *in situ* XRD results (inset) suggest that the average structure remains $B2$ spanning over the whole transition temperature range. These results indicate that no normal martensitic transformation occurs (neither $B19$ nor $9R$ martensite). Thus, the $Ti_{50}(Pd_{41}Cr_9)$ alloy of invariance bears the crystalline $B2$ cubic structure, but indeed undergoes a strain glass transition with T_0 at 298 K [13].
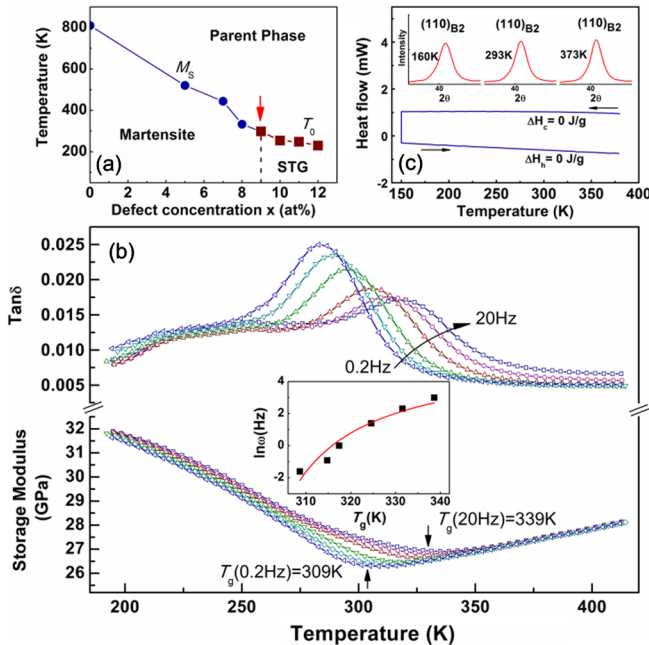
FIG. 1 (color online).   (a) The phase diagram of $Ti_{50}(Pd_{50-x}Cr_x)$ as proposed in Ref. [13]. The vertical arrow indicates the composition of the sample used. (b) DMA results demonstrate that it undergoes a dynamic freezing transition, which is manifested by the frequency dispersion of the storage modulus dip temperature T_g and internal friction peak temperature. Inset of (b) shows fitting of $T_g(\omega)$ by the Vogel-Fulcher relation, where the ideal freezing temperature is $T_0 = 298$ K. (c) DSC results show that no obvious endothermic or exothermic peak and *in situ* XRD results [inset of (c)] show the average $B2$ structure is kept to temperature well below T_0.

After twin-jet electropolishing [18], the sample was taken to the HREM observation by JEOL 2100F microscopy. The HREM micrographs characterizing the local structure of a frozen strain glass state at 293 K (below T_0) are shown in Fig. 2. The diffraction pattern in the inset of Fig. 2(a) was obtained from the $[1\bar{1}1]_{B2}$ zone axis. Its fundamental pattern keeps the right hexangular symmetry, which indicates the average structure being the same as the $B2$ parent phase, in accordance with the XRD results shown in the inset of Fig. 1(c). Even though the average symmetry does not change, there are incommensurate 1/3 reflections lying along the $\langle 10\bar{1}\rangle^*$ direction, indicating the phonon softening of the TA_2 branch [19–21]. Similar observations have been reported in defect-doped TiPd-based alloys, and they considered such incommensurate reflections to come from the incommensurate phase (IC phase) [22,23]. The IC phase may also occur before martensitic transformation in many shape memory alloys and was thought to be a premartensite state [24,25]. A very recent study has shown that the premartensite state or IC phase can be linked to the concept of strain glass, being the unfrozen or frozen state of a strain glass (see details in Ref. [26]). In the present work, one of the incommensurate reflections was circled to get the dark field image shown in Fig. 2(a). The image shows that nanosized domains are randomly distributed in the matrix, which is similar with Sarkar's results on $Ti_{48.5}Ni_{51.5}$ strain glass alloy [4]. However, the domain shape is irregular in the present study, contrasting with the spherical domains in the $Ti_{48.5}Ni_{51.5}$ alloy [4]. Such similar irregular nanosized domains were also found in the $Ti_{50}(Pd_{34}Fe_{16})$ alloy [27]. This contrasting domain shape can be attributed to the fact that the anisotropic factor of TiPd-based systems is much larger than that of TiNi-based systems [28].

A high resolution TEM picture (using a large aperture) of the square area in Fig. 2(a) was then obtained in Fig. 2(b) to reveal the lattice image of the frozen strain glass state more clearly. The image was obtained from the $[1\bar{1}1]_{B2}$ incident direction. The modulated nanodomains can be identified in the image, as marked by domain A and domain B in Fig. 2(b). The domain size is estimated to be several to several tens of nanometers with irregular shape, which is in accordance with what has been observed in the dark field image in Fig. 2(a). Besides these nanosized domains, there exist some regions without obvious modulation, as circled in Fig. 2(b) between domain A and B. It seems to suggest the existence of a $B2$-like structure in certain nanosized regions and the modulated domains are separated by these $B2$-like regions. But more investigation (like a through focus series technique [29]) is needed to check whether these $B2$-like regions are undistorted or not.

Figure 2(c) is the enlarged image of the square area in Fig. 2(b), so that the local ordering of frozen strain glass state can be illustrated more clearly. It is known that the basal plane shuffle (110) $[1\bar{1}0]$ leads to the lattice modulation in a TiPd alloy [30]. In our sample, the modulated
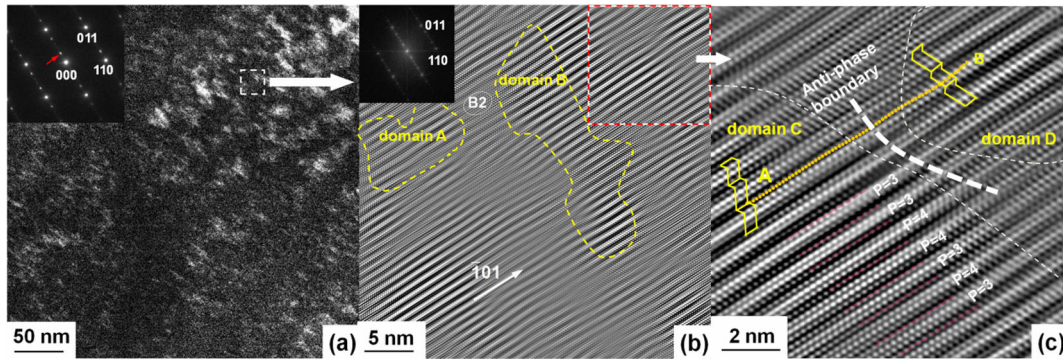
FIG. 2 (color online).   (a) The dark field image of $Ti_{50}(Pd_{41}Cr_9)$ at room temperature (293 K) obtained by using the reflection at the incommensurate 1/3 position in the inset of (a). (b) High resolution TEM image of the square area in Fig. 2(a) obtained from the incident zone and the inset is the fast Fourier transform pattern. (c) The enlarged image from the square area in (b), where the antiphase boundary can be seen between two neighboring domains, and the modulation periods in each domain are inhomogeneous, i.e., a combined stacking period of three and four plane intervals [represented by $P = 3$ and $P = 4$ in Fig. 2(c)].

stacking period varies from place to place in the strain glass state; i.e., it can be either three or four as shown in Fig. 2(c). Therefore, the "unit cell" within each domain cannot be repeated periodically over the entire lattice and it is such mixing of the stacking period (3 and 4 plane intervals) that gives rise to the incommensurate 1/3 reflections in diffraction patterns. Therefore, the exact local strain order in $Ti_{50}(Pd_{41}Cr_9)$ strain glass is shuffle induced nanosized domains with a mixture of stacking periods of 3 and 4 plane intervals. This is different from an ideal $9R$ martensite (with stacking period of 3) found in this system.

Based on the above results and analysis, here we provide the ball-and-stick model to illustrate the transformation behaviors in TiPd-based alloys. For the binary Ti-Pd alloy without Cr doping, it is the $B2$ phase at the temperature higher than M_s and the corresponding crystal structure is shown in Fig. 3(a). Upon martensitic transformation, the $(110)_{B2}$ plane of the parent phase shuffles along the $[\bar{1}10]$ direction, resulting in three kinds of more close-packed planes $(001)_M$, as indicated by A, B, C in Fig. 3(a). Usually, the three types of atomic planes are stacked with a period of three in the sequence of "$ABCBCACAB$." Such martensitic transformation in the Ti-Pd alloy can be illustrated by the lattice change from Figs. 3(b) to 3(c), seen from the [001] direction.

After doping sufficient Cr to substitute Pd (larger than 9 at %), the shuffle induced strain glass transition occurs instead of the normal martensitic transformation. Two domains of strain glass and their boundary are illustrated in Fig. 3(d). Previous studies have suggested that the coupling between defect-induced strain and the phonon softening gives rise to the distorted areas in the transformed systems [25]. The doped Cr atoms here with smaller atomic radius serve as point defects to substitute the original Pd atoms. Consequently, the doped Cr atoms will distort the host lattice, as shown in Fig. 3(d). For the area where the defect concentration is high, the lattice is distorted badly. As a result, the shuffle process will not occur and the distorted $B2$ phase will be kept to low temperature in that

area, as indicated by the yellow color in Fig. 3(d). The defect induced distortions thus hinder the long range shuffle process. For instance, as shown in Fig. 3(d), the atom plane A in modulated domain A does not extend to the modulated domain B; instead, due to the distortions induced by Cr atoms the plane becomes sequence C in the
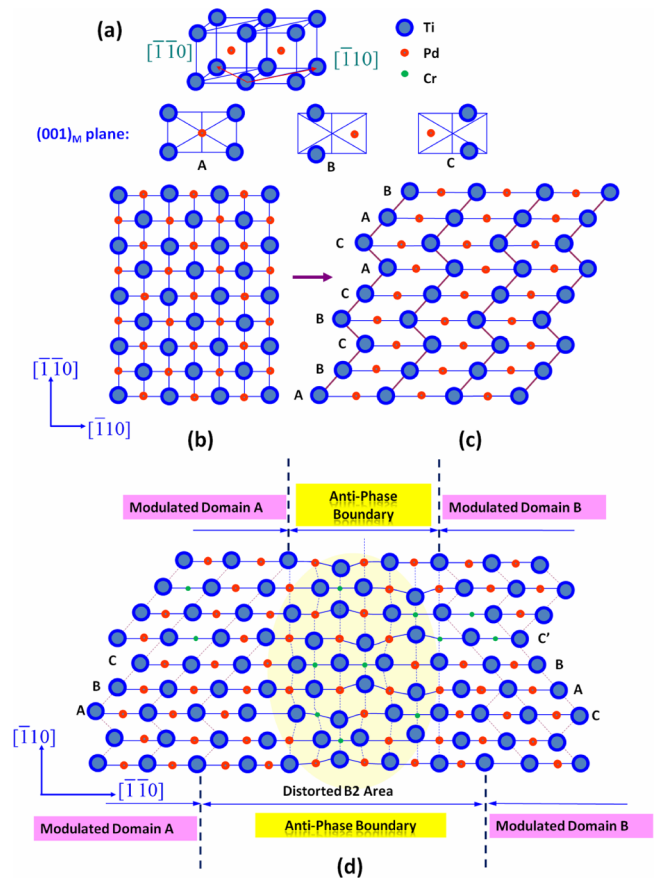
FIG. 3 (color online).   Ball-and-stick model for the martensitic transformation and strain glass transition in the Cr-free and Cr-doped Ti-Pd system, respectively (see details in the text).

neighboring domain B. Thus, the modulated nanosized martensite domains in strain glass are hardly able to grow and kept to be nanosized in the frozen strain glass state. And the sequence of the stacking in neighboring domains is not the same and is likely to be antiphase related. After the neighbored domains are self-accommodated by the antiphase relationship, the average structure of strain glass still keeps $B2$ cubic. Moreover, the defects can modify the modulation period to four or even more. As shown in Fig. 3(d), the stacking sequence in domain B is $CABC'$ (where C' is slightly different from C due to the lattice distortion by Cr substitutions). Such mixture of the modulation period explains why the superlattice reflection locations deviate from the $1/3$ position in the diffraction pattern.

The key features observed in Fig. 2(c) seem to be consistent with the above schematic model. We draw two "unit cells" by considering the regular slip in every third basal plane in two neighboring domains C and D, respectively, as indicated by the solid yellow lines in Fig. 2(c). It is noted that the unit cells are not unique within each domain, as the stacking intervals varies from place to place. We found that the unit cell of the two neighboring domains C and D have opposite shuffle direction. The boundary between the two strain domains with different atomic shuffle directions is a kind of "antiphase boundary" [31–33]. However, the precise amount of shuffle in the unit cell requires higher resolution images and image simulations using multislice or other algorithms [29,34].

After characterizing the exact local structure of frozen strain glass in the $Ti_{50}(Pd_{41}Cr_9)$ alloy, the key question now is how the local structure evolves during the freezing process of strain glass transition. The *in situ* HREM observation upon cooling throughout the strain glass transition is shown in Fig. 4. The ideal freezing temperature (T_0) of this alloy is around 298 K and our observation is performed at four different temperatures, 473, 393, 333, and 293 K. The insets in Fig. 4 are the corresponding diffraction pattern to each lattice image. At 473 K ($T_0 + 175$ K) [Fig. 4(a)], which is far from T_0, the lattice is mostly the undistorted B2 structure and only very slight lattice distortion can be seen, as indicated by the circled area. Correspondingly, besides the fundamental reflection spots, the incommensurate reflection spots are invisible in the diffraction pattern. With temperature decreasing to 393 K ($T_0 + 95$ K) [Fig. 4(b)], there are some cross-hatched "tweedlike" patterns distributed in the matrix, as indicated by the circled area, which has been expected as sticky strain liquid in Ref. [26]. Accordingly, some slight incommensurate reflection spots can be seen in the diffraction pattern. On further cooling to 333 K ($T_0 + 35$ K) [Fig. 4(c)], the size of modulation streaks increases comparing with that at 393 K and this characterizes the growth of modulated domains on cooling. At the same time, the intensity of incommensurate reflection spots is enhanced. Such results are helpful for understanding the
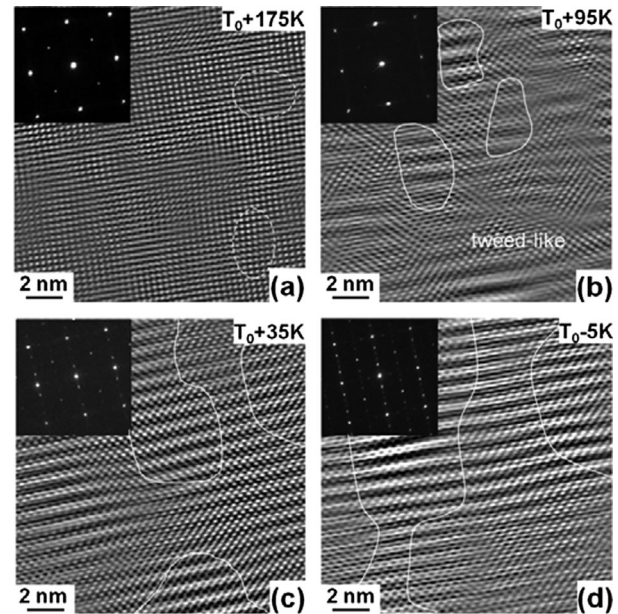
FIG. 4   *In situ* HREM observation on the $Ti_{50}(Pd_{41}Cr_9)$ strain glass alloy at (a) 473, (b) 393, (c) 333, and (d) 293 K, with the corresponding diffraction patterns shown in each inset, respectively. With temperature decreasing, the nanosized domains become larger and more populated, and the corresponding incommensurate inflections are enhanced.

long-standing "incommensurate phase" or "modulated structure" in defect-containing alloys above M_s [24,25,35]. The premartensitic phase is considered to be static as observed by TEM while dynamic measurements demonstrate it is ergodic (dynamic) [26]. Figures 4(b) and 4(c) show that there indeed exists a portion of long lived "distorted" or "modulated" areas, which appears as a quasistatic tweed pattern (or nanodomains) but without breaking the global ergodicity above M_s. At 293 K ($T_0 - 5$K) [Fig. 4(d)], we can see the crystal lattice is mostly composed of nanosized domains with modulations and the corresponding reflection spots are even more enhanced than that at 333 K. That is in accordance with the dark field image of the frozen strain glass state shown in Fig. 2(a). Thus, Fig. 4 vividly suggests the freezing process of strain glass is associated with the formation, growth, and finally being frozen of nanosized domains with inhomogeneous modulations and, correspondingly, the appearance and enhancement of incommensurate reflections on cooling.

Figure 4 shows clearly the growth of the nanodomain in size and the increase in the volume fraction of nanodomains upon cooling. Then the mechanical response during DMA measurement can be understood. With temperature decreasing from the high temperature [Fig. 4(a)], nanodomains of different size are formed and become more populated, as shown in Figs. 4(b) and 4(c). These nanodomains with various size and inhomogeneous modulations have different relaxation time and response to the ac stress field of different frequency. This gives the strong frequency dispersion of

dynamic properties. The decrease of the storage modulus with temperature above T_g is caused by the lattice softening, while its increase below T_g can be attributed to the gradual freezing of nanodomains. Practically, the local order parameter (shuffle or strain) is likely coupled to the external stress, electric, and magnetic fields; as a result, the formation, size, and population of nanodomains are tunable by the above mentioned external fields. Such tunability may lead to a range of potential applications of strain glass alloys.

We note that Schryvers *et al.* has recently made HREM observation for a $Ti_{48.3}Ni_{51.7}$ strain glass alloy at room temperature, which is more than 150 K above its glass transition temperature [36]. Their lattice image show slight local lattice distortions being similar with our Fig. 4(a), which is taken at 175 K above the glass transition temperature of our alloy. To obtain crucial information about the evolution of local lattice distortions and their relation with martensite, it is important to perform *in situ* HREM observation over a wide temperature range spanning the glass transition temperature T_g. Our work served this purpose and provides such information.

To summarize, we obtained direct evidence of the frozen strain glass state in the $Ti_{50}(Pd_{41}Cr_9)$ alloy by HREM. The modulated shuffle in nanosized domains characterizes the inhomogeneous local ordering by combined stacking periods of three- and four-plane intervals. Nanosized domains are antiphase boundaries related. *In situ* HREM results on cooling demonstrate that the nanodomains become larger and more populated, and the corresponding incommensurate reflections are enhanced. Such direct observation of the exact local structure and its evolution with temperature provides the fundamental basis for understanding the macroscopic properties of strain glass.

---

[*] To whom all correspondence should be addressed.
Xuedezhen@mail.xjtu.edu.cn

[†] Dingxd@mail.xjtu.edu.cn

[‡] Ren.xiaobing@nims.go.jp

[1] J. A. Mydosh, *Spin Glasses: An Experimental Introduction* (Taylor & Francis, New York, 1993).

[2] E. K. H. Salje, *Phase Transitions in Ferroelastic and Co-Elastic Crystals* (Cambridge University Press, Cambridge, England, 1990).

[3] K. Otsuka and C. M. Wayman, *Shape Memory Materials* (Cambridge University Press, Cambridge, England, 1998).

[4] S. Sarkar, X. Ren, and K. Otsuka, Phys. Rev. Lett. **95**, 205702 (2005).

[5] D. Wang, Y. Wang, Z. Zhang, and X. Ren, Phys. Rev. Lett. **105**, 205702 (2010).

[6] Y. Wang, X. Ren, K. Otsuka, and A. Saxena, Phys. Rev. B **76**, 132201 (2007).

[7] Y. Wang, X. Ren, and K. Otsuka, Phys. Rev. Lett. **97**, 225703 (2006).

[8] R. Vasseur, T. Lookman, and S. R. Shenoy, Phys. Rev. B **82**, 094118 (2010).

[9] R. Vasseur and T. Lookman, Phys. Rev. B **81**, 094107 (2010).

[10] Y. Wang, X. Song, X. Ding, S. Yang, J. Zhang, X. Ren, and K. Otsuka, Appl. Phys. Lett. **99**, 051905 (2011).

[11] Y. Ji and X. Ren (unpublished).

[12] Y. Zhou, D. Xue, X. Ding, Y. Wang, J. Zhang, Z. Zhang, D. Wang, K. Otsuka, J. Sun, and X. Ren, Acta Mater. **58**, 5433 (2010).

[13] Y. Zhou, D. Xue, X. Ding, K. Otsuka, J. Sun, and X. Ren, Appl. Phys. Lett. **95**, 151906 (2009).

[14] S. Semenovskaya and A. G. Khachaturyan, Acta Mater. **45**, 4367 (1997).

[15] S. David, J. Phys. Condens. Matter **20**, 304213 (2008).

[16] P. Lloveras, T. Castan, M. Porta, A. Planes, and A. Saxena, Phys. Rev. Lett. **100**, 165707 (2008).

[17] R. Vasseur, D. Xue, Y. Zhou, W. Ettoumi, X. Ding, X. Ren, and T. Lookman Phys. Rev. B **86**, 184103 (2012).

[18] The TEM specimens were prepared by electrothinning in a twin-jet apparatus using a solution of 80 vol% CH_3OH and 20 vol% H_2SO_4 and operating at 30 V at a temperature of 250 K.

[19] P.-A. Lindgård and O. G. Mouritsen, Phys. Rev. Lett. **57**, 2458 (1986).

[20] A. Gonzàlez-Comas, E. Obradó, L. Mañosa, A. Planes, V. Chernenko, B. Hattink, and A. Labarta, Phys. Rev. B **60**, 7085 (1999).

[21] A. Planes, L. Mañosa, and E. Vives, Phys. Rev. B **53**, 3039 (1996).

[22] K. Enami, K. Horii, and Y. Kitano, in *Proceedings of the Materials Research Society International Meeting on Advanced Materials*, edited by K. Otsuka and K. Shimizu (MRS, Warrendale, PA, 1989), Vol. 90, p. 117.

[23] K. Enami, K. Horii, and J. Takahashi, ISIJ Intl. **29**, 430 (1989).

[24] L. E. Tanner, A. R. Pelton, G. Van Tendeloo, D. Schryvers, and M. E. Wall, Scr. Metall. Mater. **24**, 1731 (1990).

[25] S. M. Shapiro, B. X. Yang, Y. Noda, L. E. Tanner, and D. Schryvers, Phys. Rev. B **44**, 9301 (1991).

[26] X. Ren *et al.*, Philos. Mag. **90**, 141 (2010).

[27] Y. Murakami, S. Kidu, and D. Shindo, J. Phys. (Paris) **112**, 1031 (2003).

[28] S. Shapiro, G. Xu, B. Winn, D. Schlagel, T. Lograsso, and R. Erwin, Phys. Rev. B **76**, 054305 (2007).

[29] D. Schryvers, and L. E. Tanner, Ultramicroscopy **32**, 241 (1990).

[30] A. J. Schwartz, S. Paciornik, R. Kilaas, and L. E. Tanner, J. Microsc. **180**, 51 (1995).

[31] M. Matsuda, T. Hara, and M. Nishida, Mater. Trans., JIM **49**, 461 (2008).

[32] M. Matsuda, K. Kuramoto, Y. Morizono, S. Tsurekawa, E. Okunishi, T. Hara, and M. Nishida, Acta Mater. **59**, 133 (2011).

[33] N. Yamamoto, K. Yagi, and G. Honjo, Phys. Status Solidi A **44**, 147 (1977).

[34] T. Wim and D. Schryvers, Nat. Mater. **8**, 752 (2009).

[35] S. M. Shapiro, J. Z. Larese, Y. Noda, S. C. Moss, and L. E. Tanner, Phys. Rev. Lett. **57**, 3199 (1986).

[36] D. Schryvers, S. Cao, S. Pourbabak, H. Shi, and J. B. Lu, J. Alloys Compd. **577**, S705 (2013).